The Retinal Proteome in Experimental Diabetic Retinopathy

UP-REGULATION OF CRYSTALLINS AND REVERSAL BY SYSTEMIC AND PERIOCULAR INSULIN*[S]

Patrice E. Fort‡§, Willard M. Freeman¶, Mandy K. Losiewicz‡, Ravi S. J. Singh‡, and Thomas W. Gardner‡‖****

Diabetic retinopathy is the leading cause of blindness in working age persons. Targeted studies have uncovered several components of the pathophysiology of the disease without unveiling the basic mechanisms. This study describes the use of complementary proteomic and genomic discovery methods that revealed that the proteins of the crystallin superfamily are increased dramatically in early diabetic retinopathy. Orthogonal methods confirmed that the amplitude of the up-regulation is greater than other changes described so far in diabetic retinopathy. A detailed time course study during diabetes showed differential up-regulation of the different isoforms of the crystallins superfamily. α- and β-crystallins were regulated primarily at the translation level, whereas γ-crystallins were also regulated transcriptionally. We also demonstrated cell-specific patterns of expression of the different crystallins in normal and diabetic rat retinas. In addition, systemic and periocular insulin treatments restored retinal crystallin protein expression during diabetes, indicating effects of phosphoinositide 3-kinase/Akt activity. Altogether this work shows the importance of proteomics discovery methods coupled with targeted approaches to unveil new disease mechanistic details and therapeutic targets. ***Molecular & Cellular Proteomics 8: 767–779, 2009.***

Diabetic retinopathy is the leading cause of blindness in working age persons, and despite numerous studies, the pathophysiological mechanisms, especially during the early stages of diabetes, remain to be elucidated. Diabetic retinopathy develops, to some degree, in nearly all patients with diabetes and is the most common cause of new cases of blindness among adults. The predominant causes of vision loss are clinically significant macular edema and proliferative diabetic retinopathy, but vision impairment can be prevented or minimized if the retinopathy is identified in its early stages. Diabetic retinopathy includes microvascular and neuronal, glial, and microglial cell defects early in the course of the disease before clinically visible vascular lesions. Photoreceptor and ganglion cell death occurs as early as 2–4 weeks after the onset of diabetes (1–3).

Because of the difficulty of studying the mechanisms of the early stages of diabetes in humans, rodent models of type 1 and type 2 diabetes have been developed. Those models have been used to study various specific aspects of early stages of diabetic retinopathy including blood retinal barrier leakage (4), growth factor signaling such as the insulin/insulin-like growth factor receptor and vascular endothelial cell receptor pathways (5, 6), and oxidative stress mechanisms such as reactive oxygen species and advanced glycation end product production (7, 8). These targeted studies provide valuable information on different aspects of the pathology and are useful in new therapeutic development, but more detailed discovery research is also needed to understand the full range of metabolic dysregulation that leads to diabetes complications. Proteome profiling using two-dimensional (2D)[1] DIGE and/or isobaric tag for relative and absolute quantitation (iTRAQ) are methods that can characterize new pathophysiological components and potential therapeutic targets.

Several studies have used 2D DIGE to gain a better understanding of diabetic complications in the heart and retina (9–12). These global approaches revealed biochemical changes in the retina including changes in the expression of αA- and αB-crystallin proteins. Crystallins were described originally as lens-specific structural proteins and are now recognized in multiple tissues. There are two main crystallin gene families, the α-crystallins and the β/γ-crystallins. α-Crystallins belong to the small heat shock protein family and prevent aberrant protein interactions and/or degradation and regulate apoptosis (13–16). The functions of the γ- and β-crystallins are less clear, although like the α family they are involved in chaperone activity, apoptosis regulation, and vascular remodeling in the retina (17, 18).

Here we report the use of two complementary discovery methods, 2D DIGE and iTRAQ, followed by validation and

From the Departments of ‡Ophthalmology, ¶Pharmacology, and ‖Cellular and Molecular Physiology, Penn State College of Medicine, Hershey, Pennsylvania 17033

Received, July 21, 2008, and in revised form, October 31, 2008

Published, MCP Papers in Press, December 1, 2008, DOI 10.1074/mcp.M800326-MCP200

[1] The abbreviations used are: 2D, two-dimensional; iTRAQ, isobaric tag for relative and absolute quantitation; STZ, streptozotocin; GFAP, glial fibrillary acidic protein; mRNA, messenger ribonucleic acid; INL, inner nuclear layer; GCL, ganglion cell layer; NFL, nerve fiber layer; SCX, strong cation exchange; NCBI, National Center for Biotechnology Information.

© 2009 by The American Society for Biochemistry and Molecular Biology, Inc.
This paper is available on line at http://www.mcponline.org

TABLE I

Summary of the weight, blood glucose (BG), and number of animals (n) prior to sacrifice for the different groups of control, diabetic, and insulin-treated diabetic animals used for this study

	Diabetes duration														
	1 week			2 weeks			4 weeks			8 weeks			12 weeks		
	n	BG	Weight	*n*	BG	Weight	*n*	BG	Weight	*n*	BG	Weight	*n*	BG	Weight
		mg/dl	*g*		*mg/dl*	*g*		*mg/dl*	*g*		*mg/dl*	*g*		*mg/dl*	*g*
Control	16	82 ± 9	222 ± 13	16	86 ± 3	213 ± 12	24	69 ± 7	359 ± 45	24	84 ± 9	479 ± 26	24	80 ± 9	551 ± 56
Diabetic	20	280 ± 117	199 ± 15	14	392 ± 60	181 ± 16	26	367 ± 67	280 ± 62	24	486 ± 47	287 ± 38	24	435 ± 80	299 ± 68
Diabetic + systemic insulin				14	339 ± 34	198 ± 15	20	154 ± 103	335 ± 11	24	142 ± 105	404 ± 26	20	310 ± 106	447 ± 61
Diabetic + local insulin										8	445 ± 81	271 ± 44			
Diabetic + systemic and local insulin										4	141 ± 47	391 ± 15			

in-depth characterization using targeted methods. We found with both proteomics methods a rapid and dramatic increased expression of α-, β-, and γ-crystallin isoforms in the retina of diabetic animals. We also describe the cellular topology of the crystallins and the ganglion cell-specific expression of the γ-crystallins up-regulated in retina during diabetes. Finally we show that the increased crystallin expression is differentially regulated between the isoforms at transcriptional and translational levels.

EXPERIMENTAL PROCEDURES

Induction of Diabetes and Insulin Therapies—Age-matched male Sprague-Dawley rats (Charles River) were used in all experiments. Rats were housed under a 12-h light/dark cycle with free access to a standard rat chow and water. All experiments were conducted in accordance with the Association for Research in Vision and Ophthalmology Resolution on the Care and Use of Laboratory Animals. Diabetes was induced by intraperitoneal injection of streptozotocin (STZ) (65 mg/kg; Sigma) dissolved in sodium citrate buffer, pH 4.5, and control rats received equivalent volumes of buffer alone as described previously (1) (Table I). STZ-injected rats were considered diabetic when exhibiting blood glucose levels >13.9 mmol/liter (250 mg/dl) within 5 days after diabetes induction (One-Touch meter, Lifescan, Milpitas, CA). Continuous insulin therapy was administered during the second half of the duration of diabetes by implanting a subcutaneous insulin pellet to deliver ~2 units of bovine insulin/day for the duration of the experiment (LinShin Canada, Toronto, Ontario, Canada) (1). A second implant was given after 4 weeks for longer studies. Acute, short term insulin therapy consisted of a daily injection of 5 units of Humulin Regular, 5 units of Humulin Ultralente for 4 days before the animals were killed. Subconjunctival insulin (15 μl of a 100 nmol/liter solution of bovine crystalline insulin (Sigma)) was injected in one eye, and vehicle (PBS with 0.1% BSA) was injected in the other eye under ketamine (4 mg/kg)/xylazine (0.4 mg/kg) anesthesia. This dose was chosen on the basis of preliminary studies showing activation of the retinal insulin receptor signaling pathway without affecting blood glucose levels (data not shown). The 4-, 8-, and 12-week diabetes duration studies were chosen because they lead to increased neuronal cell death, microvascular leakage, astrocyte defects, microglial cell activation, and impaired insulin receptor signaling (1, 4, 19–21). Before death, rats were anesthetized with injection of 100 mg/kg sodium pentobarbital intraperitoneally and killed by decapitation following motor reflex loss for rapid dissection of retinas. Retinas were immediately frozen in liquid nitrogen and stored at −80 °C until analysis (see below).

2D Gels—Quantitative 2D DIGE was performed as detailed previously (22). All 2D DIGE methods and results are provided in minimum information about a proteomics experiment-gel electrophoresis (MIAPE-GE)-compliant form. Retinas were homogenized in lysis buffer (10 mM HEPES, 42 mM KCl, 5 mM $MgCl_2$, 0.1 mM EDTA, 0.1 mM EGTA, 50 mM sodium pyrophosphate, 1 mM dithiothreitol, 1 mM phenylmethylsulfonyl fluoride, 1 mM Na_3VO_4, 10 mM NaF, 10 mM benzamidine, 10% glycerol, 1% Nonidet P-40, and one protease inhibitor tablet/10 ml) by sonication as described previously (6). Protein concentrations were measured with the Pierce BCA reagent, and all samples were adjusted for equal protein concentration. Retinal samples were purified from lipids and nucleic acids by precipitation (2D-Cleanup, GE Healthcare) and quantified by using the 2D-Quant protein assay (GE Healthcare). Samples were brought to a pH between 8.0 and 9.0, and 50 μg of each sample were labeled using Cy3 or Cy5 dye (GE Healthcare); 200 μg of unlabeled protein was used for a preparative/picking gel for MS identification of protein species. Samples were focused on 24-cm, pH 3–10 IEF gels (GE Healthcare) and separated by molecular weight on 10% polyacrylamide gels. On completion of electrophoresis, the picking gel was stained with SYPRO Ruby (Bio-Rad), and all gels were imaged on a Typhoon 9410 scanner (GE Healthcare). Analysis of gel images was performed using DeCyder 6.0 software (GE Healthcare) to detect spots and calculate relative expression value.

MALDI-TOF/TOF Mass Spectrometry—MALDI-TOF/TOF mass spectrometry was performed as described previously (22). Spots shown to be differentially regulated were removed from the picking gels using a robotic Ettan Spot Picker (GE Healthcare), and gel plugs were subjected to in-gel trypsin digestion and ZipTip (Millipore, Bedford, MA) desalting. 0.9 μl of sample from each gel plug was spotted onto a 384-position MALDI target followed by 0.8 μl of α-cyano-4-hydroxycinnamic acid. Protein identifications were performed in a peptide mass fingerprinting approach (MS and MS/MS) using an Applied Biosystems 4800 MALDI-TOF/TOF instrument. The instrument was calibrated with Applied Biosystems Calibration Mixture 1. Measurements were taken in the positive ion mode between 800 and 4000 *m/z* with a signal to noise filter of 10, mass exclusion tolerance of 0.2 Da, and peak density filter of 50 peaks/200 Da. The 10 most intense ions with a minimum signal to noise of 75 that were not included on an exclusion list containing trypsin autolysis, matrix, and tryptic peptides of human keratin were subjected to MS/MS. MS/MS was performed without collision-induced decay in a mass range from 60 to 20 Da below the precursor mass with a fragment tolerance of 0.2 Da for +1 charged ions. Data interpretation was performed using GPS Explorer (version 3.6) and database searching was carried out using Mascot (version 2.0.00). Database searches were carried out against the *Rattus* subset of the NCBI database downloaded on February 16, 2008 (107,758 entries searched). As all studies were conducted with only rat retinal samples, only the *Rattus* taxonomy was used. In the final combined MS and MS/MS database searches,

identifications required a confidence interval of greater than 95%. When multiple isoforms of the protein were identified the isoform with the highest confidence interval that met one of the following criteria was reported: 1) had an identified peptide exclusive to that isoform or 2) the gel spot location matched the theoretical molecular weight and pI.

iTRAQ Analysis—Eightplex iTRAQ was conducted on 100 μg of sample in 20 μl of 0.5 M triethylammonium bicarbonate, pH 8.5. Samples were then denatured and reduced by bring the samples to final concentrations of 0.01% SDS and 5 mM tris(2-carboxyethyl)phosphine. Sample were incubated at 60 °C for 1 h, brought to a concentration of 3.65 mM iodoacetamide, and incubated for 30 min at room temperature, protected from light. Samples were then trypsin-digested with 0.01 mg of sequence grade trypsin (Promega) overnight at 48 °C overnight (12–16 h). Digests were then labeled with the appropriate iTRAQ reagent for 2 h and then quenched by addition of 100 μl of water. All of the different samples were then combined followed by three rounds of vacuum drying and resuspension.

The mixture was reconstituted in 500 μl of 12 mM ammonium formate, 25% acetonitrile, pH 2.75 for SCX liquid chromatographic separation. SCX separations were performed on a passivated Waters 600E HPLC system using a 4.6 $\times$-250 mm PolySULFOETHYL Aspartamide column (PolyLC, Columbia, MD) at a flow rate of 1 ml/min. Buffer A contained 10 mM ammonium formate, pH 3.6 in 20% acetonitrile, 80% water. Buffer B contained 666 mM ammonium formate, pH 3.6 in 20% acetonitrile, 80% water. The gradient was Buffer A at 100% (0–30 min following sample injection), 0 $\rightarrow$ 35% Buffer B (30–48 min), 35 $\rightarrow$ 100% Buffer B (48–49 min), 100% Buffer B (49–56 min), and then at 56 min switched back to 100% A to re-equilibrate for the next injection. The first 28 ml of eluant (containing all flow-through fractions) were combined into one fraction, and then 14 additional 2-ml fractions were collected. All 15 of these SCX fractions were dried down completely to reduce the volume and to remove the volatile ammonium formate salts, then resuspended in 15 μl of 2% (v/v) acetonitrile, 0.1% (v/v) trifluoroacetic acid, and filtered prior to reverse phase C_{18} nanoflow-LC separation.

For second dimension separation by reverse phase nanoflow LC, each SCX fraction was autoinjected onto a Chromolith CapRod column (150 $\times$ 0.1 mm; Merck) using a 5-μl injector loop on a Tempo LC MALDI Spotting system (ABI/MDS Sciex). Buffer C was 2% acetonitrile, 0.1% trifluoroacetic acid, and Buffer D was 98% acetonitrile, 0.1% trifluoroacetic acid. The elution gradient was 100% C (0–4 min), 0 $\rightarrow$ 10% D (4–10 min), 10 $\rightarrow$ 25% D (10–30 min), 25 $\rightarrow$ 40% D (30–35 min), 40 $\rightarrow$ 80% D (35–38 min), 80% D (38–42 min), 80 $\rightarrow$ 0% D (42–43 min), and 0% D (43–50 min). The flow rate was 3 μl/min, and an equal flow of MALDI matrix solution was added postcolumn (7 mg/ml recrystallized α-cyanohydroxycinnamic acid, 2 mg/ml ammonium phosphate, 0.1% trifluoroacetic acid, 80% acetonitrile).

The combined eluant was automatically spotted onto a stainless steel MALDI target plate every 6 s (0.6 μl/spot) for a total of 370 spots per original SCX fraction. MALDI target plates (15 per experiment) were analyzed in a data-dependent manner on an ABI 4800 MALDI TOF-TOF instrument. Both MS and MS/MS default calibrations were performed at the start of analysis of each plate using the peaks from the Applied Biosystems Calibration Mixture 1 for the MS calibrations (13 spots) and the MS/MS fragment peaks of the Glu-fibrinogen peptide contained in that calibration mixture for the MS/MS calibration (five spots). MS spectra were acquired from each sample spot (500 laser shots/spot) in the positive ion mode between 800 and 4000 *m/z* with peaks chosen with a signal to noise ratio of at least 10 and a peak density filter of 50 peaks/200 Da. A plate-wide interpretation was then performed to select peaks for MS/MS analysis such that MS/MS was run only on the best representative of each distinct *m/z* value seen across multiple spots.

MS/MS was performed with collision-induced decay of selected peaks, collecting data in the mass range from 60 Da below the precursor mass with a fragment tolerance of 0.2 Da for +1 charged ions. MS/MS accumulation was stopped after at least eight peaks had a signal to noise ratio of 100 or higher or when 2500 total laser shots were accumulated for each MS/MS spectrum.

Protein identification and quantitation were performed using the Paragon algorithm as implemented in Protein Pilot 2.0 software (ABI/MDS Sciex). Database searches were carried out against the *Rattus* subset of the NCBI database downloaded on July 22, 2008 (109,096 entries searched) concatenated with a reversed "decoy" version. Confident protein identifications required a ProteinPilot unused score of at least 1.3 (95% confidence interval) and a local false discovery rate estimation of no higher than 5%. The local false discovery rate estimation was calculated from the slope of the accumulation of decoy database hits using the Proteomics System Performance Evaluation Pipeline software from Tang *et al.* (23).

Immunoblot Analysis—Retinal lysates were prepared as described for 2D gel analysis to proceed to validation using immunoblot analysis with antibodies directed against α-, β-, and γ-crystallins generously provided by Dr. Samuel Zigler. Immunoblots were performed as described previously but using 4–12% NuPAGE gels (24) and MES buffer following the manufacturer's instructions. Results were normalized by reprobing the same membrane using an antibody against actin (Millipore).

Immunohistochemistry—Immunohistochemistry was performed as described previously (5). Briefly eyecups were embedded in optimum cutting temperature compound and snap frozen in dry ice cooled with 2-methylbutane directly after enucleation. Sections (10 μm) from each experimental group were mounted on the same slide. The slides were blocked with donkey serum before primary antibody incubations at 4 °C overnight. Antibodies against crystallins were the same ones used for immunoblotting (see above); double labeling was done using anti-vimentin (Neomarker), anti-neurofilament 200 kDa (Sigma), and anti-GFAP (Chemicon). Cyanine 3- or cyanine 5-conjugated secondary antibodies were used (Jackson ImmunoResearch Laboratories).

RNA Isolation and Real Time PCR—Total RNA was isolated with TRI Reagent/bromochloropropane (Molecular Research Center, Cincinnati, OH) following standard methods (25), and quality and quantity were assessed using the RNA 6000 Nano LabChip with an Agilent 2100 Expert Bioanalyzer (Agilent, Palo Alto, CA). Quantitative PCR analysis was performed as described previously (26). Briefly quantitative PCR was performed using the 7900HT Sequence Detection System (Applied Biosystems, Foster City, CA), 384-well optical plates, and Assay-On-Demand (Applied Biosystems) gene-specific primers and probes. ABI SDS 2.2.2 software and the $2^{-\Delta\Delta Ct}$ analysis method were used to quantify relative amounts of product using β-actin as an endogenous control. β-Actin levels were determined to be unchanged in an absolute quantification experiment (data not shown).

Statistical Analysis—For all experiments, the data were normalized to the actin signal as control before analysis. Analysis of variance models with heterogeneous variances, adjusted for the replication of the experiment, were fit to the data to assess differences between STZ-induced diabetic rats with or without insulin treatment and control rats. The means $\pm$ S.E. and statistical tests are reported. Analyses were performed using non-repeated measures analysis of variance followed by Student-Newman-Keuls test for multiple comparisons.

RESULTS

Diabetes Increases Retinal Crystallin Protein Expression—We used the 2D DIGE and gel analysis method on protein extracts from 8-week diabetic animals and their age-

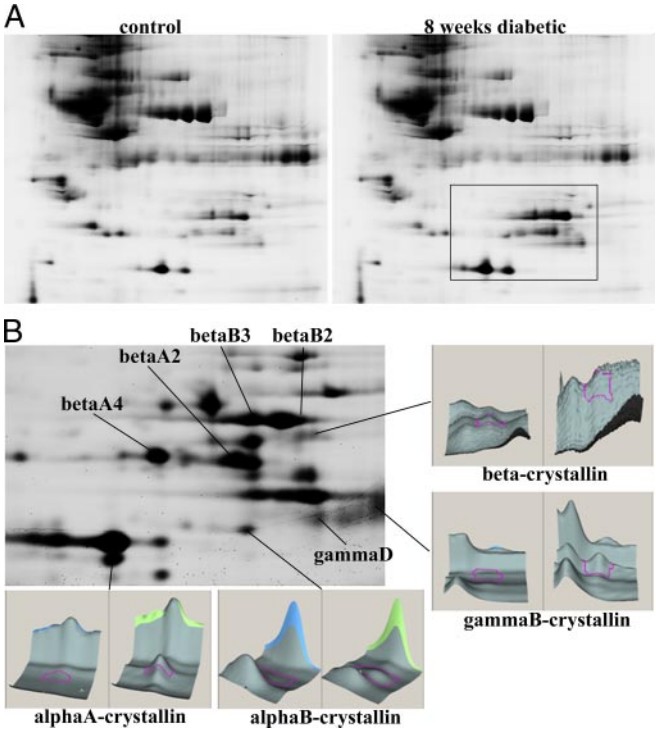

FIG. 1. *A*, representative 2D DIGE images of the retinal proteome from control and 8-week diabetic rats. *B*, image of the region of the picking gel corresponding to the *inset* visualized in *A* with a representative example of three-dimensional reconstruction of the crystallin spots identified in MS in control and diabetic rats.

matched controls ($n = 4$) to generate proteome maps of diabetic and non-diabetic rat retina with or without insulin treatment. The use of 10% gels and a pH range of 3–10 revealed altered expression of more than 30 proteins. Nine of the proteins showed a 2.1–44.2-fold increased expression, although most of the changes revealed decreased protein expression in the diabetic state. Interestingly those nine proteins were concentrated in a region of the gels corresponding to a range between 19 and 30 kDa and a pH between 5 and 8 (Fig. 1). Tandem mass spectrometry analysis of the spots from this region revealed that the up-regulated proteins correspond to different proteins or isoforms of the crystallin family. Statistical analysis of the proteome differential expression during diabetes revealed that all the crystallin protein members identified during this study were overexpressed in diabetic animals. Members of both families of crystallin, α-crystallins (αA and αB) and $\beta\gamma$-crystallins (βA2, βA3, and βB4; γB and γD) were overexpressed up to 18-fold during the course of diabetes (Table II). These increases are particularly striking given that global retinal protein synthesis at this same time point was decreased by 33%.[2] Increased expression of the members of the α-crystallin family was demonstrated previously in STZ diabetic rats (27), but this is the first time that members of the $\beta\gamma$-crystallin family were also shown to be increased. Fig. 2 shows that iTRAQ analysis confirmed the increased crystallin expression observed in the retina during diabetes. To the best of our knowledge, changes in crystallin expression are the largest and most consistent retinal protein changes observed in experimental diabetes.

Time Course Study of the Crystallin Protein Up-regulation during Diabetes—To confirm the quantification and identification of the crystallin overexpression during diabetes, immunoblots were performed using pan-specific antibodies against α-, β-, and γ-crystallins, and quantification of the signal was performed by normalizing to actin content. Crystallins were detected at various levels in all control animals. Although a statistically significant increase in α- and γ-crystallins expression was detected in retinas from 8-week diabetic rats (Fig. 3, *A* and *C*), the increased level of expression of β-crystallins reached statistical significance only after 12 weeks of diabetes (Fig. 4*B*). This difference between the results obtained by immunoblot and proteome analysis is probably related to the fact that the antibodies recognize multiple isoforms from the same subfamily, whereas 2D analysis separates individual isoforms. Additionally the confirmatory methods compress different isoforms with dissimilar isoelectric points into one band on a one-dimensional SDS-PAGE gel. This is a common challenge with confirmation of proteomics experiments, and novel methods will have to be used to explore these post-translational modifications.

To better understand the possible implications of increased crystallin expression, we studied the time-dependent expression of the different crystallins during diabetes. This detailed time course study during the early phase of diabetes onset showed that both the α- and β-crystallins have a biphasic up-regulation of their expression during diabetes (Fig. 4, *A* and *B*). Whereas up-regulation of α-crystallins expression was detected at 2 and 8 weeks of diabetes separated by a level of expression similar to control at 4 weeks, β-crystallins were up-regulated as early as 1 week after diabetes before returning to control levels after only 2 weeks. Up-regulation of β-crystallin expression was then detected again at 8 weeks of diabetes. By contrast, γ-crystallins were constantly up-regulated between 4 and 12 weeks after the onset of diabetes, increasing in a logarithmic fashion (Fig. 4*C*). This time course study also points out the difference in the levels of up-regulation of the different crystallins during diabetes. Although both the α- and β-crystallin expression levels were doubled, the γ-crystallin levels of expression were increased over 8-fold after 12 weeks of diabetes. These disparities between the crystallins point out their distinct functions and cellular localization.

Crystallin Protein Cellular Localization in Normal and Diabetic Rat Retinas—To examine the cellular localization of the different crystallins in the retina of diabetic and control rats, we performed an immunohistochemical study on retinal sections from control and 8-week diabetic rats using the same pan-specific antibodies used for immunoblot analysis.

[2] P. E. Fort, M. K. Losiewicz, S. A. Kimball, L. S. Jefferson, and T. W. Gardner, manuscript in preparation.

TABLE II
Crystallin proteins identified in rat retina by MS using the 2D DIGE method and their relative changes in diabetes

Protein name	NCBI accession number	Average ratio (diabetic/control)	Peptide count	Protein score	Confidence interval	Coverage
					%	%
α-Crystallin A chain	NP_036666	44.27	5	225	100	30
α-Crystallin A chain	NP_036666	18.4	6	301	100	35.8
α-Crystallin A chain	NP_036666	2.78	8	308	100	51.4
α-Crystallin A chain	NP_036666	2.05	8	215	100	52.6
α-Crystallin B chain	Q80X03	9.72	4	92	99.9	28
α-Crystallin B chain	Q80X03	2.51	8	222	100	54.8
α-Crystallin B chain	Q80X03	17.1	6	102	100	44
α-Crystallin B chain	Q80X03	1.41	10	302	100	60
β-Crystallin A2	Q8CGQ0	2.16	7	293	100	44.6
β-Crystallin A2	Q8CGQ0	1.82	6	106	100	37
β-Crystallin A4	NP_113877	2.27	9	326	100	75.5
β-Crystallin A4	NP_113877	2.17	8	198	100	65.8
β-Crystallin B1	NP_037068	1.59	7	132	100	38.3
β-Crystallin B2	NP_037069	19.89	5	60	97.8	26.3
β-Crystallin B2	NP_037069	2.48	11	253	100	55.6
β-Crystallin B3	Q9JJU9	1.85	10	224	100	55.9
γ-Crystallin B	P10066	15.53	6	126	100	37.7
γ-Crystallin D	P10067	2.38	5	89	99.9	33.9

Positive immunoreactivity for α-crystallins was observed in the photoreceptor segments and outer limiting membrane, the outer plexiform layer, and the ganglion cell/nerve fiber layer (GCL/NFL) of normal animals (Fig. 5*A*). Whereas colocalization was observed when double labeled with a vascular cell marker (Fig. 5*A*, *higher magnification*, *arrows*), no colocalization was evident when double labeled with an astrocyte-specific marker (Fig. 5*A*, *higher magnification*, *arrowheads*). Signal intensity was increased in diabetes almost exclusively in the GCL/NFL (Fig. 5*A*, *bottom*). Higher magnification images show increased α-crystallin immunoreactivity in diabetic retina around the blood vessels of the GCL/NFL as well as in the activated Müller glial cells (Fig. 5*A*, *long arrows*) but not in the astrocytes (Fig. 5*A*, *arrowheads*).

β-Crystallin immunoreactivity was mainly observed in the ganglion cell layer, a subset of the nuclei of the inner nuclear layer (INL) and the photoreceptor segments (Fig. 5*B*). Cell bodies immunolabeled in the INL did not colocalize with a Müller glial cell marker suggesting that β-crystallins are expressed by a subset of bipolar, amacrine, or horizontal cells (Fig. 5*B*, *higher magnification*, *arrows*). Double immunostaining with a nerve fiber layer marker (neurofilament N52) and an astrocyte marker (GFAP; data not shown) did not show any colocalization, indicating that the β-crystallin staining observed in the GCL does not correspond to the axons of the ganglion cells or the astrocytes. A slight increase of the overall immunoreactivity was observed on sections from diabetic rat retinas with particular increase of the intensity observed in some nuclei of the INL (Fig. 5*B*,

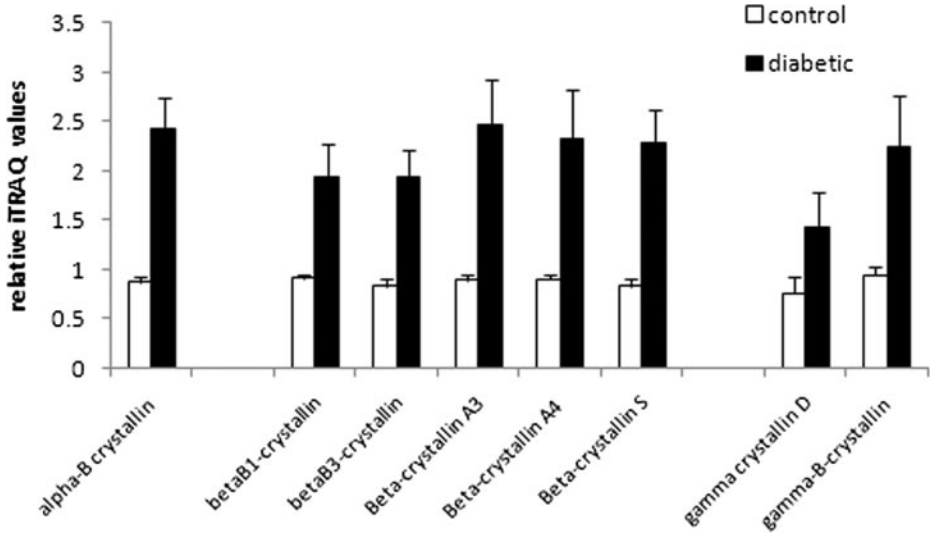

FIG. 2. **Crystallin proteins identified in rat retina by iTRAQ and their relative changes in diabetes.** Protein expression is presented as relative to that of the control ($n = 3$/group).

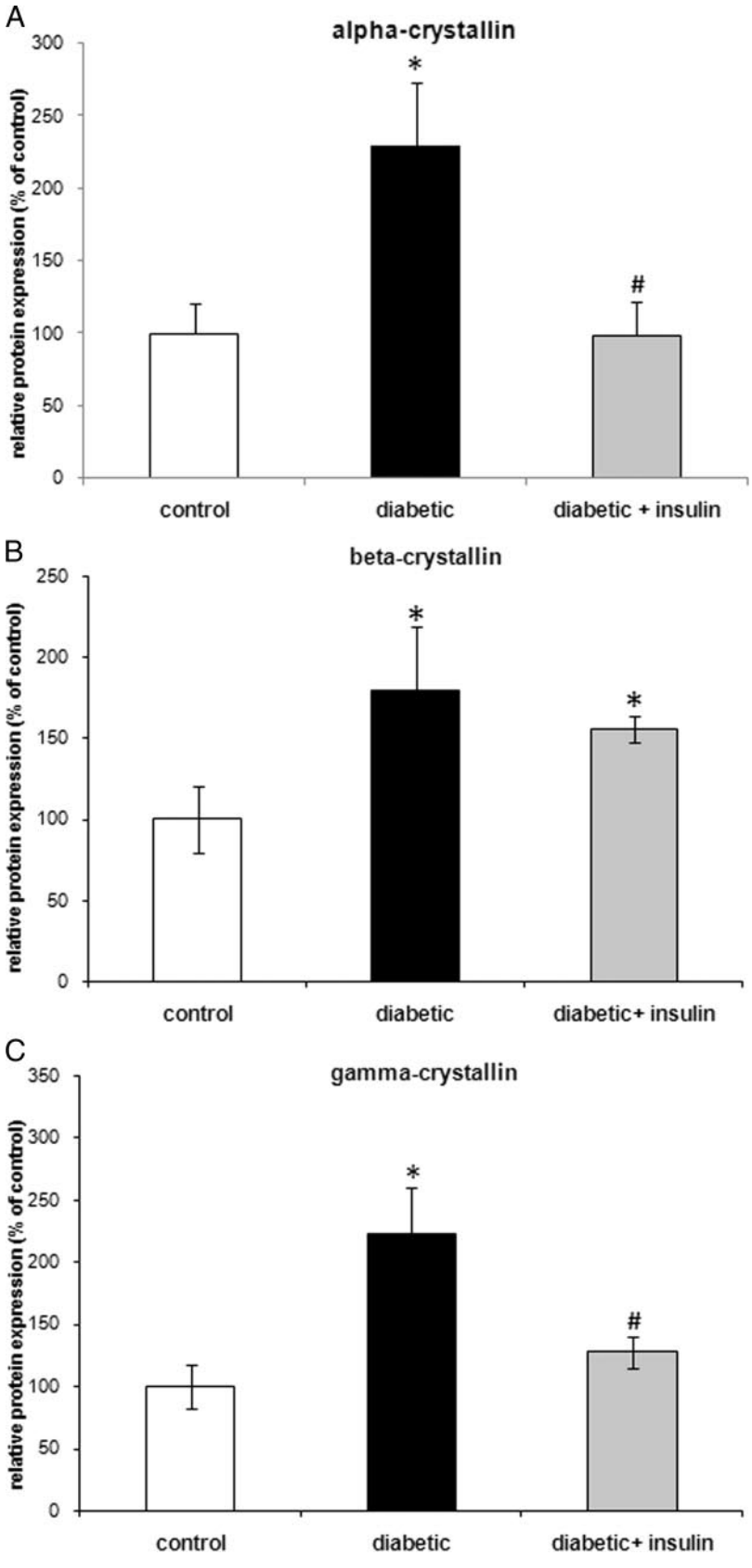

FIG. 3. **Western blot confirmation of 2D proteomics and iTRAQ data.** Graphic representations of the relative protein quantification of α-crystallins (*A*), β-crystallins (*B*), and γ-crystallins (*C*) are shown. $n = 8$/group; *, significantly different from control ($p < 0.05$). #, significantly different from diabetic ($p < 0.05$). Data are means $\pm$ S.E.M.

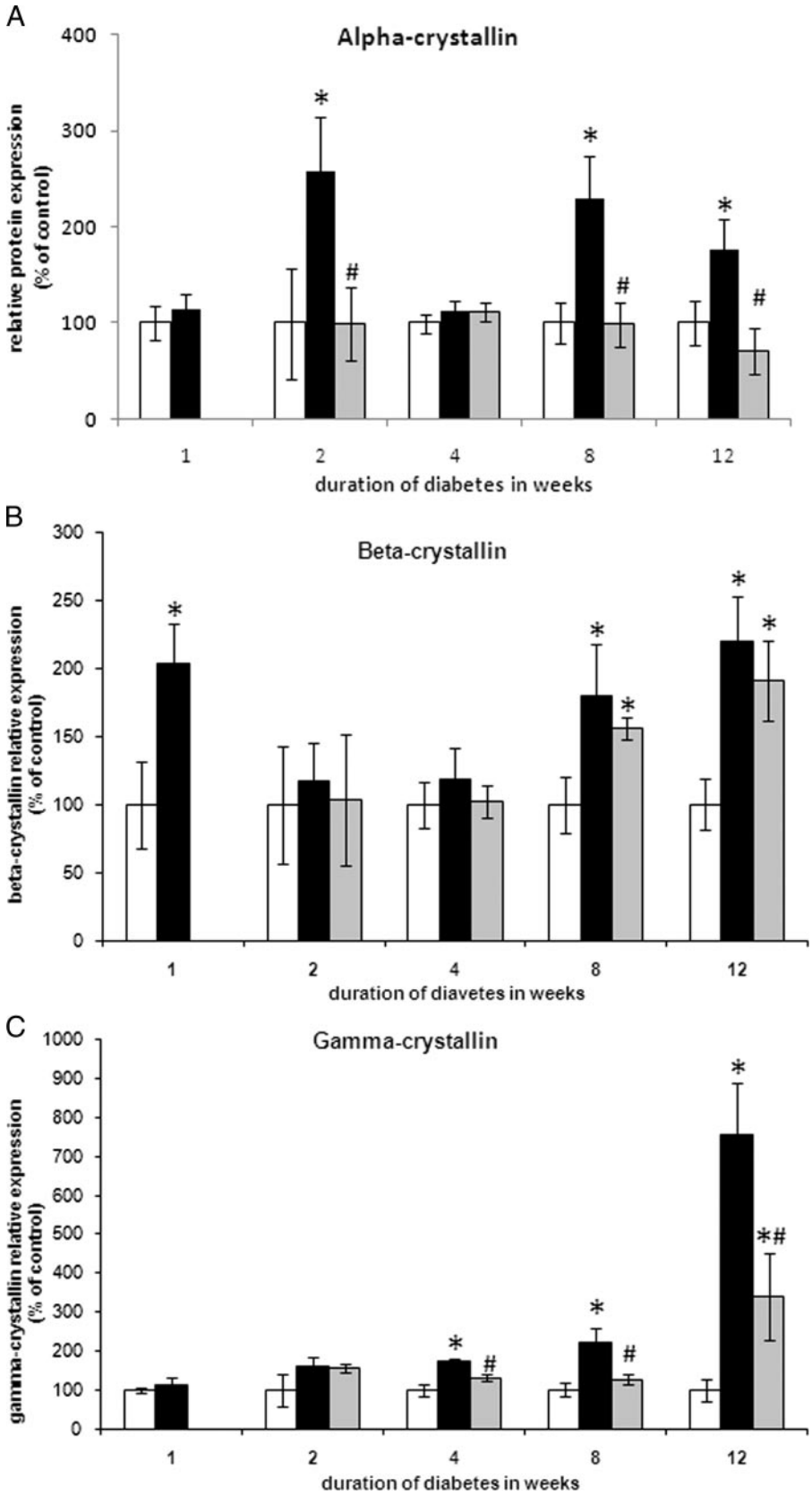

FIG. 4. **Time course of the relative quantification of the expression of α-crystallins (*A*), β-crystallins (*B*), and γ-crystallins (*C*) during early stages of diabetes between control (*white*), diabetic (*black*), and diabetic with systemic insulin (*gray*).** $n = 8$/group; *, significantly different from control ($p < 0.05$); #, significantly different from diabetic ($p < 0.05$).

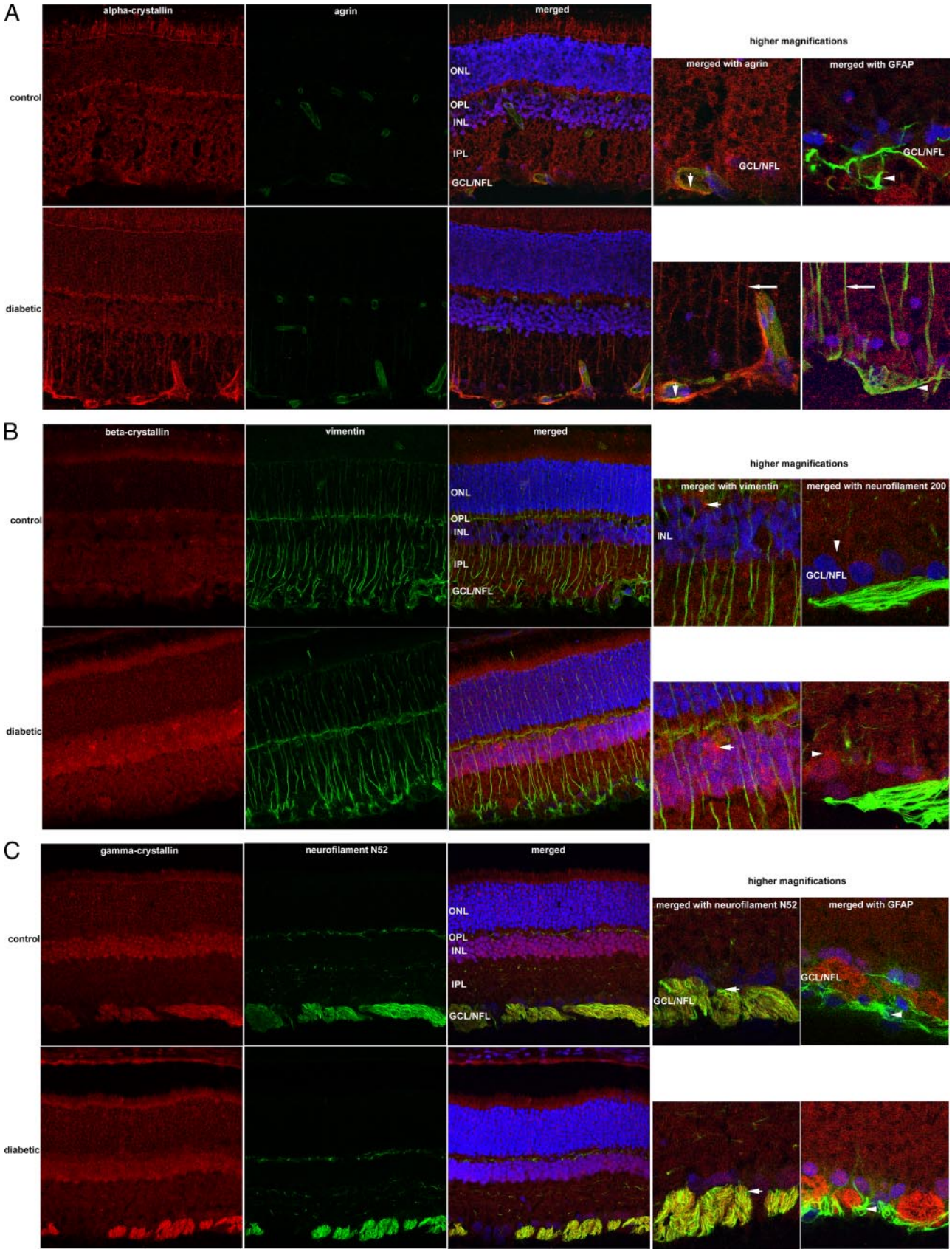
A
alpha-crystallin
agrin
merged
higher magnifications
merged with agrin
merged with GFAP
control
ONL
OPL
INL
IPL
GCL/NFL
GCL/NFL
GCL/NFL
diabetic
B
beta-crystallin
vimentin
merged
higher magnifications
merged with vimentin
merged with neurofilament 200
control
ONL
OPL
INL
IPL
GCL/NFL
INL
GCL/NFL
diabetic
C
gamma-crystallin
neurofilament N52
merged
higher magnifications
merged with neurofilament N52
merged with GFAP
control
ONL
OPL
INL
IPL
GCL/NFL
GCL/NFL
GCL/NFL
diabetic

TABLE III
Crystallin mRNAs identified in rat retina by microarray and their relative changes in diabetes (n = 6/group)

Gene name	Gene symbol	NCBI accession number	-Fold changes (diabetic/control)
Crystallin, ζ	*Cryz*	CB616233	0.55
Crystallin, βA2	*Cryba2*	NM_173140	1.93
Crystallin, αB	*Cryab*	NM_012935	2.01
Crystallin, αA4	*Cryba4*	NM_031689	2.39
Crystallin, βB3	*Crybb3*	NM_031690	2.40
Crystallin, βB1	*Crybb1*	NM_012936	2.71
Crystallin, γB	*Crygb*	BG371963	11.19

higher magnification, *arrows*) and the GCL (Fig. 5*B*, *higher magnification*, *arrowheads*).

γ-Crystallins immunoreactivity was observed in the GCL/NFL, the INL, and the photoreceptors segments (Fig. 5*C*). The very intense immunoreactivity observed in the GCL/NFL co-localized with a nerve fiber marker indicating that γ-crystallins are expressed prominently in the ganglion cell axons (Fig. 5*C*, *higher magnification*, *arrows*). Increased immunoreactivity was observed in the GCL/NFL retinal layer of diabetic rats (Fig. 5*C*, *bottom left*). Higher magnification images show that the immunoreactivity observed in the GCL/NFL is particularly specific to the ganglion cell axons (Fig. 5*C*, *higher magnification*, *arrows*) and not the astrocytes (Fig. 5*C*, *higher magnification*, *arrowheads*). Together the increased crystallin expression patterns in retinal neurons point to a role in the prominent response of metabolically active neurons to the stresses of insulin-deficient diabetes.

Time Course Study of Crystallin mRNA Levels during Diabetes—Crystallins are regulated at the transcriptional level in the lens (28), so we studied the expression level of crystallin mRNAs using microarrays and specific real time RT-PCR methods to determine whether the up-regulation of the crystallins observed in diabetes was transcriptionally mediated. We have previously reported whole genome gene expression assessment of retinal mRNA at 4 and 12 weeks of diabetes (46). Transcriptomics data revealed that crystallin transcript levels were among the most up-regulated mRNAs after 12 weeks of diabetes in the STZ rat model (Table III). RT-quantitative PCR validation was performed using primers specific for αA-, αB-, βA4-, βA3-, and γD-crystallins. We found that both αA- and αB-crystallin mRNAs were not statistically significantly up-regulated in retinas of diabetic animals at either 4 or 12 weeks after the onset of diabetes (Fig. 6*A*). Both βA4- and βB3-crystallins showed a lot of variability but no statistically significant changes at either 4 or 12 weeks of diabetes (Fig. 6*B*). γD-Crystallin messenger showed an increased level of over 3- and 16-fold, respectively, 4 and 12 weeks after the onset of diabetes (Fig. 6*C*). This up-regulation is more than 2-fold the protein increase observed at 4 and 12 weeks for γ-crystallins suggesting that there are multiple levels of crystallin regulation in the retina.

Impact of Insulin Treatment on Crystallin Expression during Diabetes—Systemic insulin administration using subcutaneous implants reversed hyperglycemia and prevented weight loss induced by diabetes (Table I). We showed previously that basal retinal insulin receptor signaling is impaired in diabetes (6) so we followed the effects of insulin therapy on retinal crystallin expression in the same diabetic rat model. Systemic insulin administration prevented or partially reversed the up-regulation of both α- and γ-crystallins (Figs. 3 and 4, *A* and *C*) but did not prevent or reverse the β-crystallin up-regulation (Fig. 4*B*). Because the insulin implants were implanted only for the second half of the duration of diabetes, the results obtained for γ-crystallins represent a reversal of the up-regulation or prevention of further increase that could explain the partial recovery at the 12-week time point. Also systemic insulin administration could be restoring the levels of crystallins by normalizing the glycemia and/or via a direct effect of the insulin therapy. Intraocular insulin restores insulin receptor kinase activity without affecting blood glucose levels (6) so we tested the hypothesis that a local insulin administration could also correct the crystallin up-regulation. Subconjunctival very low dose insulin for the last 4 days of the study did not reduce the blood glucose level (Table I) but did reverse the up-regulation of both α- and γ-crystallins observed after 8 weeks of diabetes (Fig. 7). When rats were given insulin both systemically and locally, we observed an additive effect of the treatments except for β-crystallins, which remained unchanged with both treatments. These results imply that diabetes-induced up-regulation of α- and γ-crystallins is sensitive to retinal specific insulin receptor action as well as the systemic metabolic state consistent with previous findings that systemic and local insulin administration restores insulin receptor signaling via the prosurvival phosphoinositide 3-kinase/Akt pathway (6).

DISCUSSION

We compared the retinal proteome and genome of control and diabetic rats; the comparison revealed the overexpres-

FIG. 5. **Immunolocalization of retinal crystallin proteins in normal and 8-week diabetic rats.** *A*, α-crystallin immunolocalization in control and diabetic retina double labeled with a marker of the blood vessels (agrin). Higher magnification images of double immunolabeling of α-crystallins with agrin or GFAP (astrocyte marker) are shown on the *right side* of the panel. *B*, β-crystallin immunolocalization in control and diabetic retina double labeled with a Müller glial cell marker (vimentin). Higher magnification images of double immunolabeling of β-crystallins with vimentin or neurofilament N52 (ganglion cell axon marker) are shown on the *right side* of the panel. *C*, γ-crystallin immunolocalization in control and diabetic retina double labeled with a ganglion cell axon marker (neurofilament N52). Higher magnifications of double immunolabeling of γ-crystallins and neurofilament N52 or GFAP are shown on the *right side* of the panel. *ONL*, outer limiting membrane; *OPL*, outer plexiform layer; *IPL*, inner plexiform layer.

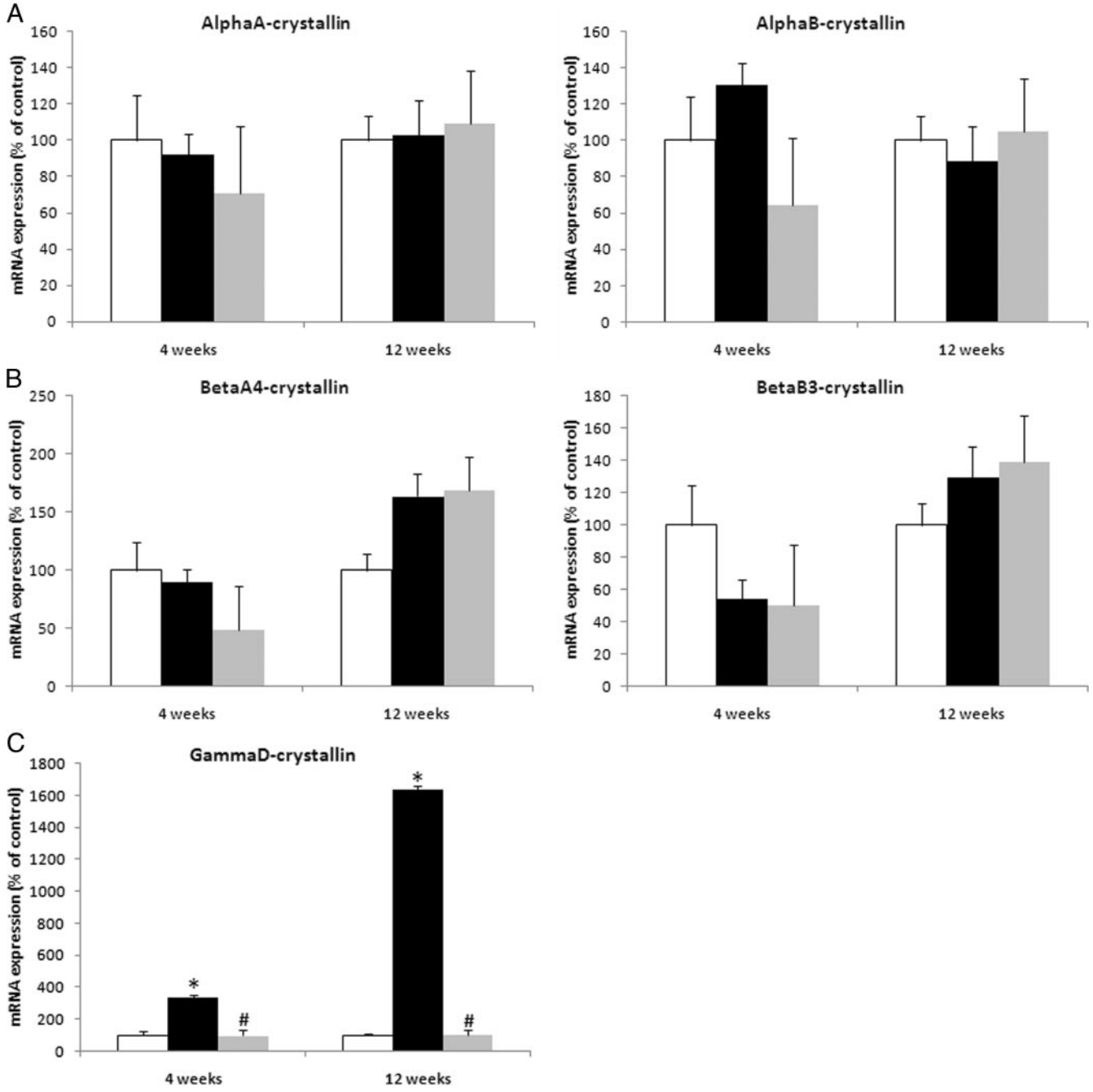

FIG. 6. **Relative expression of the transcripts of αA- and αB- (*A*), βA4- and βB3- (*B*), and γD-crystallins (*C*) in the retina from control and diabetic rats ($n \geq 25$/group) with or without insulin systemic administration.** *, significantly different from control ($p < 0.05$); #, significantly different from diabetic ($p < 0.05$).

sion of multiple isoforms of the crystallin family during diabetes. The major findings reported are as follows. 1) α-, β-, and γ-crystallin isoforms are overexpressed with diabetes. This was observed by two proteomics discovery methods (2D DIGE and iTRAQ) and confirmed by immunoblotting. Despite the commonality of increased expression of the isoforms, the time and spatial pattern of expression differ among the different subfamilies. 2) Previous reports have shown an up-regulation of both αA- and αB-crystallins in STZ-induced diabetic rats after 8 weeks of diabetes (27), but this is the first report of an up-regulation of isoforms of the β/γ-crystallin protein family during diabetes. 3) This is also the first time- and cell-specific study of the expression of the crystallins in the retina in a disease state such as diabetes. 4) This work shows that both systemic and local insulin administration can reverse diabetes-induced retinal perturbations like crystallin up-regulation.

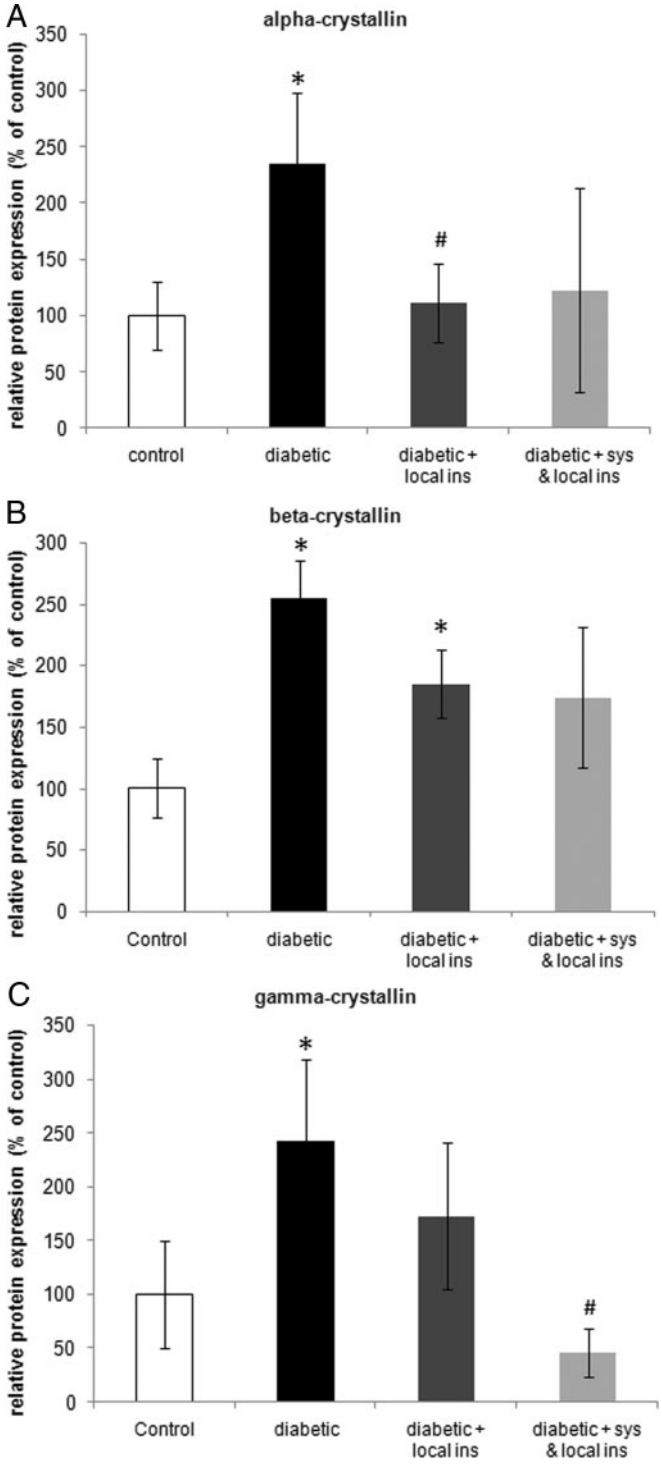

FIG. 7. **Relative quantification of the expression of α-crystallins (*A*), β-crystallins (*B*), and γ-crystallins (*C*) in the retina from diabetic rats treated with systemic (*sys*) or local insulin (*ins*) administration.** $n = 8$/group; *, significantly different from control ($p < 0.05$); #, significantly different from diabetic ($p < 0.05$).

It has been hypothesized that the expression of crystallins in the retina results from lens contamination during the retinal dissection (29). To exclude the possibility of lens contamination, retinas were dissected under microscopic control with a careful observation of the lens integrity during the dissection. Although it is impossible to rule out that part of the signal was due to crystallins secreted by lens cells, several pieces of evidence indicate that retinal cells express crystallins. First the RT-quantitative PCR data presented in this work confirm the presence of crystallin mRNA in the retinal tissue. We also detected the expression of crystallin in primary retinal cells and different retinal cell lines (data not shown), showing clearly that retina expresses crystallin proteins. Moreover the differential retinal localization demonstrated by immunohistochemistry also strongly supports crystallin expression by retinal cells.

Crystallin expression levels are increased in other retinal injury models such as light toxicity, retinal detachment, and experimental glaucoma (30–32). α-Crystallin expression increases in drusen, a specific deposit associated with age-related macular degeneration (33, 34), whereas β-crystallin expression increases in astrocytes during retinal development (18). Despite intense staining in the inner retina for several crystallins, we showed that the up-regulation during diabetes was not in the astrocytes but more likely in the ganglion cells for the γ-crystallins and other neurons of the inner retina for the β-crystallins (Fig. 5). These results suggest that the crystallin up-regulation observed in diabetes is distinct from the glial response to retinal injury as described in several central nervous system pathologies that can include α-crystallins in astrocytes, so-called Rosenthal fibers (35).

Despite their implication in several different retinal diseases, the function(s) of the crystallin up-regulations remains to be elucidated. The crystallin up-regulation observed during diabetes develops around the same time as hallmarks of diabetic retinopathy such as increased caspase activity and vascular permeability, changes involved in neuronal cell loss and glial cell dysfunction. Retinal expression of β- and γ-crystallins has been recently related to vascular remodeling during development (36). Because diabetes induces vascular endothelial growth factor expression and increases retinal vascular leakage, it is suspected that the increased crystallin expression could be related to vascular remodeling in diabetes (18). We observed β- and γ-crystallin expression mainly in neurons, whereas α-crystallins were mostly in cells participating in the blood retinal barrier. A recent study (37) showed that β-crystallins could be secreted and exert a paracrine role on ganglion cell axon regrowth. Thus, it is possible that neuronal overexpression of crystallins could lead to crystallin secretion to promote axonal neurite regrowth. Indeed Gastinger *et al.* (38) have recently shown that diabetes increases ramification of retinal axons in the same time period examined in our study.

Several studies of uveitis showed the possible involvement of α-crystallins in the inflammatory response in the retina. Up-regulation of αA-crystallin during diabetes occurs early in the course of the disease at the same time as vimentin and

GFAP, two markers of Müller glial cells, the latter indicating an involvement of Müller cells in the disease process (39). This finding, correlated with the presence of antibodies against αB-crystallins in serum from multiple sclerosis patients and mice with experimental autoimmune encephalomyelitis (40), suggests that the up-regulation of crystallins could be involved in the inflammatory component of diabetic retinopathy.

All crystallins (α-, β-, and γ-) have been implicated in the regulation of cell death in lens epithelial cells or in cells of the central nervous system. α-Crystallins have been implicated in apoptosis regulation through sequestration of Bcl-2 (B-cell CLL/lymphoma 2) family proteins or caspase interaction (41). β-Crystallins have been implicated in the regulation of vasculature in the retina during development as well as in the axon regeneration of retinal ganglion cells (36, 37). Finally γD-crystallin is involved in the apoptotic-like mechanism leading to lens fiber denucleation (17). These results suggest that the overexpression of crystallins, especially α-isoforms, could be a protective mechanism for neurons to block apoptosis or prevent damaged protein degradation (16, 42). The role of crystallins in regulating cell fate during development and during diabetes could be part of a mechanism of sensing, sending, or diffusing the death/survival signal of injured cells for the sake of the "organ." The dramatic increase of crystallin expression observed in diabetes could (i) prevent cell death by blocking apoptosis through sequestration or (ii) diffuse cell survival signals through β-crystallin secretion.

We showed that systemic and local insulin treatment reverses α- and γ-crystallin up-regulation. We also showed that insulin treatment normalizes the activity of the retinal insulin receptor/phosphoinositide 3-kinase/Akt pathway (5, 6), suggesting that this pathway is directly or indirectly involved in the regulation of α- and γ-crystallin expression in the retina. We demonstrated that this treatment can also partially reverse the increased neuronal apoptosis observed in diabetic retinopathy, pointing out the possible implication of crystallins in the regulation of this event in diabetic retinopathy.

Additional studies to clarify the role of the different crystallins in the retina are underway. Interestingly both the 2D DIGE method (Fig. 1) and immunoblot analysis (supplemental Fig. S1) results suggest that α- and β-crystallins are subject to several post-translational modifications that might include deamination or truncation such as shown previously in the lens (43, 44). A recent study also showed that γ-crystallins could also be targeted for post-translational modifications, such as tyrosine nitration, in the retina from diabetic rats (45). Identifications of these modifications will be important to determine their function in the retina.

The results reported in this study show the importance of discovery-oriented methods such as 2D DIGE and iTRAQ methods followed by detailed specific studies for the characterization of disease mechanisms. The discovery methods used in this work also showed a reduction of expression of over 20 proteins, a finding that is currently being investigated.

Acknowledgments—We thank Dr. Samuel Zigler, the Penn State Retina Research Group, and the Penn State Hershey Eye Center for critical suggestions and the antibodies; Mandy Losiewicz for technical help; and Anne Stanley from the Penn State Mass Spectrometry Core, Robert Brucklacher and Georgina Bixler from the Penn State Functional Genomics Core, and Wendy Dunton of the Penn State Juvenile Diabetes Research Foundation Animal Core Facility.

* This work was supported by grants from the Juvenile Diabetes Research Foundation, the American Diabetes Association, and the Pennsylvania Lions Sight Conservation and Eye Research Foundation. Penn State University holds intellectual property related to the use of periocular insulin for diabetic retinopathy.

S The on-line version of this article (available at http://www.mcponline.org) contains supplemental material.

§ To whom correspondence should be addressed: Dept. of Ophthalmology, Penn State College of Medicine, 500 University Dr., H166, Hershey, PA 17033. Tel.: 717-531-6711; Fax: 717-531-0631; E-mail: pef11@psu.edu.

** The Jack and Nancy Turner Professor.

REFERENCES

1. Barber, A. J., Lieth, E., Khin, S. A., Antonetti, D. A., Buchanan, A. G., and Gardner, T. W. (1998) Neural apoptosis in the retina during experimental and human diabetes. Early onset and effect of insulin. *J. Clin. Investig.* **102,** 783–791
2. Martin, P. M., Roon, P., Van Ells, T. K., Ganapathy, V., and Smith, S. B. (2004) Death of retinal neurons in streptozotocin-induced diabetic mice. *Investig. Ophthalmol. Vis. Sci.* **45,** 3330–3336
3. Park, S. H., Park, J. W., Park, S. J., Kim, K. Y., Chung, J. W., Chun, M. H., and Oh, S. J. (2003) Apoptotic death of photoreceptors in the streptozotocin-induced diabetic rat retina. *Diabetologia* **46,** 1260–1268
4. Antonetti, D. A., Barber, A. J., Khin, S., Lieth, E., Tarbell, J. M., and Gardner, T. W. (1998) Vascular permeability in experimental diabetes is associated with reduced endothelial occludin content: vascular endothelial growth factor decreases occludin in retinal endothelial cells. Penn State Retina Research Group. *Diabetes* **47,** 1953–1959
5. Reiter, C. E., and Gardner, T. W. (2003) Functions of insulin and insulin receptor signaling in retina: possible implications for diabetic retinopathy. *Prog. Retin. Eye Res.* **22,** 545–562
6. Reiter, C. E., Wu, X., Sandirasegarane, L., Nakamura, M., Gilbert, K. A., Singh, R. S., Fort, P. E., Antonetti, D. A., and Gardner, T. W. (2006) Diabetes reduces basal retinal insulin receptor signaling: reversal with systemic and local insulin. *Diabetes* **55,** 1148–1156
7. Adamis, A. P. (2002) Is diabetic retinopathy an inflammatory disease? *Br. J. Ophthalmol.* **86,** 363–365
8. Bonnardel-Phu, E., Wautier, J. L., Schmidt, A. M., Avila, C., and Vicaut, E. (1999) Acute modulation of albumin microvascular leakage by advanced glycation end products in microcirculation of diabetic rats in vivo. *Diabetes* **48,** 2052–2058
9. Quin, G. G., Len, A. C., Billson, F. A., and Gillies, M. C. (2007) Proteome map of normal rat retina and comparison with the proteome of diabetic rat retina: new insight in the pathogenesis of diabetic retinopathy. *Proteomics* **7,** 2636–2650
10. Wang, Y. D., Wu, J. D., Jiang, Z. L., Wang, Y. B., Wang, X. H., Liu, C., and Tong, M. Q. (2007) Comparative proteome analysis of neural retinas from type 2 diabetic rats by two-dimensional electrophoresis. *Curr. Eye Res.* **32,** 891–901
11. Warda, M., Kim, H. K., Kim, N., Youm, J. B., Kang, S. H., Park, W. S., Khoa, T. M., Kim, Y. H., and Han, J. (2007) Simulated hyperglycemia in rat cardiomyocytes: a proteomics approach for improved analysis of cellular alterations. *Proteomics* **7,** 2570–2590
12. Zabel, C., Sagi, D., Kaindl, A. M., Steireif, N., Klare, Y., Mao, L., Peters, H., Wacker, M. A., Kleene, R., and Klose, J. (2006) Comparative proteomics in neurodegenerative and non-neurodegenerative diseases suggest nodal point proteins in regulatory networking. *J. Proteome Res.* **5,** 1948–1958
13. Boelens, W. C., Croes, Y., and de Jong, W. W. (2001) Interaction between αB-crystallin and the human 20S proteasomal subunit C8/α7. *Biochim.*

Biophys. Acta **1544,** 311–319
14. den Engelsman, J., Keijsers, V., de Jong, W. W., and Boelens, W. C. (2003) The small heat-shock protein αB-crystallin promotes FBX4-dependent ubiquitination. *J. Biol. Chem.* **278,** 4699–4704
15. Lin, D. I., Barbash, O., Kumar, K. G., Weber, J. D., Harper, J. W., Klein-Szanto, A. J., Rustgi, A., Fuchs, S. Y., and Diehl, J. A. (2006) Phosphorylation-dependent ubiquitination of cyclin D1 by the SCF(FBX4-αB crystallin) complex. *Mol. Cell* **24,** 355–366
16. Mao, Y. W., Liu, J. P., Xiang, H., and Li, D. W. (2004) Human αA- and αB-crystallins bind to Bax and Bcl-X_S to sequester their translocation during staurosporine-induced apoptosis. *Cell Death Differ.* **11,** 512–526
17. Wang, K., Cheng, C., Li, L., Liu, H., Huang, Q., Xia, C. H., Yao, K., Sun, P., Horwitz, J., and Gong, X. (2007) γD-crystallin associated protein aggregation and lens fiber cell denucleation. *Investig. Ophthalmol. Vis. Sci.* **48,** 3719–3728
18. Zhang, C., Gehlbach, P., Gongora, C., Cano, M., Fariss, R., Hose, S., Nath, A., Green, W. R., Goldberg, M. F., Zigler, J. S., Jr., and Sinha, D. (2005) A potential role for β- and γ-crystallins in the vascular remodeling of the eye. *Dev. Dyn.* **234,** 36–47
19. Barber, A. J., Antonetti, D. A., and Gardner, T. W. (2000) Altered expression of retinal occludin and glial fibrillary acidic protein in experimental diabetes. The Penn State Retina Research Group. *Investig. Ophthalmol. Vis. Sci.* **41,** 3561–3568
20. Reiter, C. E., Sandirasegarane, L., Wolpert, E. B., Klinger, M., Simpson, I. A., Barber, A. J., Antonetti, D. A., Kester, M., and Gardner, T. W. (2003) Characterization of insulin signaling in rat retina in vivo and ex vivo. *Am. J. Physiol.* **285,** E763–E774
21. Zeng, X. X., Ng, Y. K., and Ling, E. A. (2000) Neuronal and microglial response in the retina of streptozotocin-induced diabetic rats. *Vis. Neurosci.* **17,** 463–471
22. Freeman, W. M., Brebner, K., Amara, S. G., Reed, M. S., Pohl, J., and Phillips, A. G. (2005) Distinct proteomic profiles of amphetamine self-administration transitional states. *Pharmacogenomics J.* **5,** 203–214
23. Tang, W. H., Shilov, I. V., and Seymour, S. L. (2008) Nonlinear fitting method for determining local false discovery rates from decoy database searches. *J. Proteome Res.* **7,** 3661–3667
24. Wu, X., Reiter, C. E., Antonetti, D. A., Kimball, S. R., Jefferson, L. S., and Gardner, T. W. (2004) Insulin promotes rat retinal neuronal cell survival in a p70S6K-dependent manner. *J. Biol. Chem.* **279,** 9167–9175
25. Freeman, W. M., Nader, M. A., Nader, S. H., Robertson, D. J., Gioia, L., Mitchell, S. M., Daunais, J. B., Porrino, L. J., Friedman, D. P., and Vrana, K. E. (2001) Chronic cocaine-mediated changes in non-human primate nucleus accumbens gene expression. *J. Neurochem.* **77,** 542–549
26. Bowyer, J. F., Pogge, A. R., Delongchamp, R. R., O'Callaghan, J. P., Patel, K. M., Vrana, K. E., and Freeman, W. M. (2007) A threshold neurotoxic amphetamine exposure inhibits parietal cortex expression of synaptic plasticity-related genes. *Neuroscience* **144,** 66–76
27. Kumar, P. A., Haseeb, A., Suryanarayana, P., Ehtesham, N. Z., and Reddy, G. B. (2005) Elevated expression of αA- and αB-crystallins in streptozotocin-induced diabetic rat. *Arch. Biochem. Biophys.* **444,** 77–83
28. Cvekl, A., and Duncan, M. K. (2007) Genetic and epigenetic mechanisms of gene regulation during lens development. *Prog. Retin. Eye Res.* **26,** 555–597
29. Kamphuis, W., Dijk, F., Kraan, W., and Bergen, A. A. (2007) Transfer of lens-specific transcripts to retinal RNA samples may underlie observed changes in crystallin-gene transcript levels after ischemia. *Mol. Vis.* **13,** 220–228
30. Sakaguchi, H., Miyagi, M., Darrow, R. M., Crabb, J. S., Hollyfield, J. G., Organisciak, D. T., and Crabb, J. W. (2003) Intense light exposure changes the crystallin content in retina. *Exp. Eye Res.* **76,** 131–133
31. Vazquez-Chona, F., Song, B. K., and Geisert, E. E., Jr. (2004) Temporal changes in gene expression after injury in the rat retina. *Investig. Ophthalmol. Vis. Sci.* **45,** 2737–2746
32. Steele, M. R., Inman, D. M., Calkins, D. J., Horner, P. J., and Vetter, M. L. (2006) Microarray analysis of retinal gene expression in the DBA/2J model of glaucoma. *Investig. Ophthalmol. Vis. Sci.* **47,** 977–985
33. Johnson, P. T., Brown, M. N., Pulliam, B. C., Anderson, D. H., and Johnson, L. V. (2005) Synaptic pathology, altered gene expression, and degeneration in photoreceptors impacted by drusen. *Investig. Ophthalmol. Vis. Sci.* **46,** 4788–4795
34. Umeda, S., Suzuki, M. T., Okamoto, H., Ono, F., Mizota, A., Terao, K., Yoshikawa, Y., Tanaka, Y., and Iwata, T. (2005) Molecular composition of drusen and possible involvement of anti-retinal autoimmunity in two different forms of macular degeneration in cynomolgus monkey (Macaca fascicularis). *FASEB J.* **19,** 1683–1685
35. Head, M. W., Corbin, E., and Goldman, J. E. (1993) Overexpression and abnormal modification of the stress proteins αB-crystallin and HSP27 in Alexander disease. *Am. J. Pathol.* **143,** 1743–1753
36. Sinha, D., Klise, A., Sergeev, Y., Hose, S., Bhutto, I. A., Hackler, L., Jr., Malpic-Llanos, T., Samtani, S., Grebe, R., Goldberg, M. F., Hejtmancik, J. F., Nath, A., Zack, D. J., Fariss, R. N., McLeod, D. S., Sundin, O., Broman, K. W., Lutty, G. A., and Zigler, J. S., Jr. (2008) βA3/A1-Crystallin in astroglial cells regulates retinal vascular remodeling during development. *Mol. Cell. Neurosci.* **37,** 85–95
37. Liedtke, T., Schwamborn, J. C., Schroer, U., and Thanos, S. (2007) Elongation of axons during regeneration involves retinal crystallin βb2 (crybb2). *Mol. Cell. Proteomics* **6,** 895–907
38. Gastinger, M. J., Kunselman, A. R., Conboy, E. E., Bronson, S. K., and Barber, A. J. (2008) Dendrite remodeling and other abnormalities in the retinal ganglion cells of Ins2 Akita diabetic mice. *Investig. Ophthalmol. Vis. Sci.* **49,** 2635–2642
39. Hauck, S. M., Schoeffmann, S., Amann, B., Stangassinger, M., Gerhards, H., Ueffing, M., and Deeg, C. A. (2007) Retinal Mueller glial cells trigger the hallmark inflammatory process in autoimmune uveitis. *J. Proteome Res.* **6,** 2121–2131
40. Ousman, S. S., Tomooka, B. H., van Noort, J. M., Wawrousek, E. F., O'Conner, K., Hafler, D. A., Sobel, R. A., Robinson, W. H., and Steinman, L. (2007) Protective and therapeutic role for αB-crystallin in autoimmune demyelination. *Nature* **448,** 474–479
41. Kim, Y. H., Choi, M. Y., Kim, Y. S., Han, J. M., Lee, J. H., Park, C. H., Kang, S. S., Choi, W. S., and Cho, G. J. (2007) Protein kinase Cδ regulates anti-apoptotic αB-crystallin in the retina of type 2 diabetes. *Neurobiol. Dis.* **28,** 293–303
42. Jones, S. E., Jomary, C., Grist, J., Makwana, J., and Neal, M. J. (1999) Retinal expression of γ-crystallins in the mouse. *Investig. Ophthalmol. Vis. Sci.* **40,** 3017–3020
43. Lampi, K. J., Ma, Z., Hanson, S. R., Azuma, M., Shih, M., Shearer, T. R., Smith, D. L., Smith, J. B., and David, L. L. (1998) Age-related changes in human lens crystallins identified by two-dimensional electrophoresis and mass spectrometry. *Exp. Eye Res.* **67,** 31–43
44. Shih, M., Lampi, K. J., Shearer, T. R., and David, L. L. (1998) Cleavage of β-crystallins during maturation of bovine lens. *Mol. Vis.* **4,** 4
45. Zhan, X., Du, Y., Crabb, J. S., Gu, X., Kern, T. S., and Crabb, J. W. (2008) Targets of tyrosine nitration in diabetic rat retina. *Mol. Cell. Proteomics* **7,** 864–874
46. Brucklacher, R. M., Patel, K. M., VanGuilder, H. D., Bixler, G. V., Barber, A. J., Antonetti, D. A., Lin, C. M., LaNoue, K. F., Gardner, T. W., Bronson, S. K., and Freeman, W. M. (2008) Whole genome assessment of the retinal response to diabetes reveals a progressive neurovascular inflammatory response. *BMC Med. Genomics* **1,** 26